Journal of Southeast University (English Edition) Vol. 40, No. 1, pp. 13 - 23 Mar. 2024 ISSN 1003—7985

Vulnerability analysis of a complex super high-rise connected structure under the combined action of earthquake and wind

Lu Zheng[1,2] Yan Deyu[1] Zhou Mengyao[1] Zhao Xin[3] Zhao Yiqing[4]

([1]Department of Disaster Mitigation for Structures, Tongji University, Shanghai 200092, China)
([2]State Key Laboratory of Disaster Reduction in Civil Engineering, Tongji University, Shanghai 200092, China)
([3]Tongji Architectural Design (Group) Co., Ltd., Shanghai 200092, China)
([4]China Overseas Development Group Co., Ltd., Shenzhen 518048, China)

Abstract: To explore the design and safety performance of super high-rise connected structures under the combined action of multiple disasters, taking Suzhou Supertall as an example, a vulnerability analysis is conducted under the combined earthquake-wind actions. First, the structure's finite element model is established. Then, vulnerability assessments are conducted under individual earthquake and combined earthquake-wind actions. Finally, the response law of the structure is obtained. Results indicate that when exposed to combined earthquake-wind actions, the structure's vulnerability increases with the earthquake and wind intensities, and the seismic action dominates structural damage. The probabilities of moderate, severe, and collapse damages are higher under the combined earthquake-wind actions than those under individual earthquakes. When the wind speed reaches 40 m/s, the probabilities of the structure reaching three failure states under rare earthquakes are 99.77%, 91.56%, and 46.54%, respectively, representing an increase of 1.11%, 10.73% and 14.65% compared with those under rare earthquakes alone and an increase of 0.27%, 6.26% and 14.34% compared with those of a typical high-rise connected structure under the same combined action of disasters.

Key words: super high-rise; connected structure; multi-hazard; vulnerability; earthquake; wind load; combined action; Suzhou Supertall

DOI: 10.3969/j.issn.1003 - 7985.2024.01.002

The construction of super high-rise buildings has increased in recent years, driven by urban expansion, population concentration, and increased building density. These buildings, characterized by long service life, are inevitably subjected to various dynamic excitations, such as earthquakes and wind loads, throughout their lifecycle. As the height of the structure increases, a concomitant reduction in lateral stiffness and damping ratio occurs. Consequently, the structure becomes increasingly susceptible to the influence of wind loads[1-2]. Furthermore, owing to its long-period vibration characteristics, a high-rise structure is more vulnerable to the effects of long-period earthquakes[3-4]. Some studies indicate that during seismic events, a considerable change in atmospheric pressure often occurs, and strong winds sometimes accompany earthquakes[5-6]. Localized strong winds were observed in Tokyo under large fires after the Great Kanto Earthquake in September 1923[7]. On September 6, 2018, an earthquake of magnitude 6.7 struck Hokkaido (142.0° E, 42.7° N), coinciding with the onslaught of super typhoon "Feiyan," classified as a Category 14, on the western coast of Hokkaido (139.2° E, 43.0° N)[8]. This observation underscores the non-negligible risk associated with the simultaneous occurrence of earthquakes and strong winds. Although the likelihood of simultaneous occurrences of strong ground motion and wind load is relatively low, their concomitant impact can lead to considerably greater damage to super high-rise structures than the mere superposition of the individual effects of the two disasters[9].

Seismic vulnerability analysis allows for quantitatively assessing structural damage at different seismic intensity levels from a probabilistic perspective, which is important for evaluating the seismic safety of structures[10-12]. Incremental dynamic analysis (IDA) is one of the most widely used approaches for assessing structural performance under the influence of ground motions or wind loads. IDA is a powerful approach that relies on a series of dynamic elastic-plastic time history analyses, and the results reflect the changes in the structural system's response as load intensity varies[13-15]. Li et al.[16] investigated risk assessment and load correction methods for high-rise buildings under the combined earthquake-wind actions. They consequently revised the strength indicators in the design loads specified to guarantee structural safety. Wang[17] analyzed the multi-hazard vulnerability of high-rise frame-shear isolation structures subjected to combined wind and

Received 2023-11-06, **Revised** 2024-01-24.

Biography: Lu Zheng (1982—), male, doctor, professor, luzheng111@tongji.edu.cn.

Foundation item: National Key Research and Development Program of China (No. 2022YFC3803000).

Citation: Lu Zheng, Yan Deyu, Zhou Mengyao, et al. Vulnerability analysis of a complex super high-rise connected structure under the combined action of earthquake and wind[J]. Journal of Southeast University (English Edition), 2024, 40(1): 13 - 23. DOI: 10.3969/j.issn.1003 - 7985.2024.01.002.

earthquake effects. The results show that the coupling actions increase the probability of damage. Zhou et al.[18] used the Shanghai Tower as an example and focused on the nonlinear dynamic response and vulnerability of super high-rise structures subjected to the combined effects of an earthquake and wind. Zheng et al.[8] presented a multi-hazard-based framework to assess the damage risk of a 42-story building subjected to earthquake and wind hazards, individually and simultaneously. The Bayesian theorem was employed to derive posterior probability distributions for unknown parameters in the demand model[19–20]. A reliability-based method was applied to calculate the load modification factors of high-rise buildings subjected to seismic and along-wind loads[21]. Additionally, corrosion effects were considered factors that could potentially enhance fragility estimates for structures facing multiple hazards, including earthquakes and strong winds[22–23].

A high-rise connected structure refers to the fusion of multiple similar or dissimilar high-rise structures interconnected via corridors. Although it exhibits certain resemblances to conventional high-rise buildings, its dynamic characteristics under various disasters can substantially diverge because of the intricate nature of its design and layout. Despite several studies highlighting the performance of high-rise connected structures under the combined earthquake-wind actions, research on the coupling earthquake-wind effects on super high-rise connected structures is scarce. Yang et al.[24] conducted a multi-hazard vulnerability analysis on a high-rise connected structure under combined earthquake-wind excitations but did not further investigate complex super high-rise connected structures. Thus, the multi-hazard performance of complex super high-rise connected structures must be evaluated.

This paper takes Suzhou Supertall as an example to conduct a multi-hazard vulnerability assessment of complex super high-rise connected structures subjected to combined earthquake-wind actions. The study establishes a finite element model based on the project design, conducts a vulnerability analysis of the structure under the individual earthquake actions and under the combined earthquake-wind actions, and explores the response of the structure. Through quantitative vulnerability analysis, this study establishes a theoretical basis for the design and safety performance assessment of super high-rise connected structures under multiple hazards.

1 Project Overview

Suzhou Supertall is a 460-meter-tall structure with a three-tower reinforced concrete frame, a central core tube, and an interconnected truss system. It comprises 101 above-ground floors and 5 below-ground floors. The overall elevation and plane dimensions are displayed in Figs. 1(a) and (b). A finite element model of the structure is depicted in Fig. 1(c).

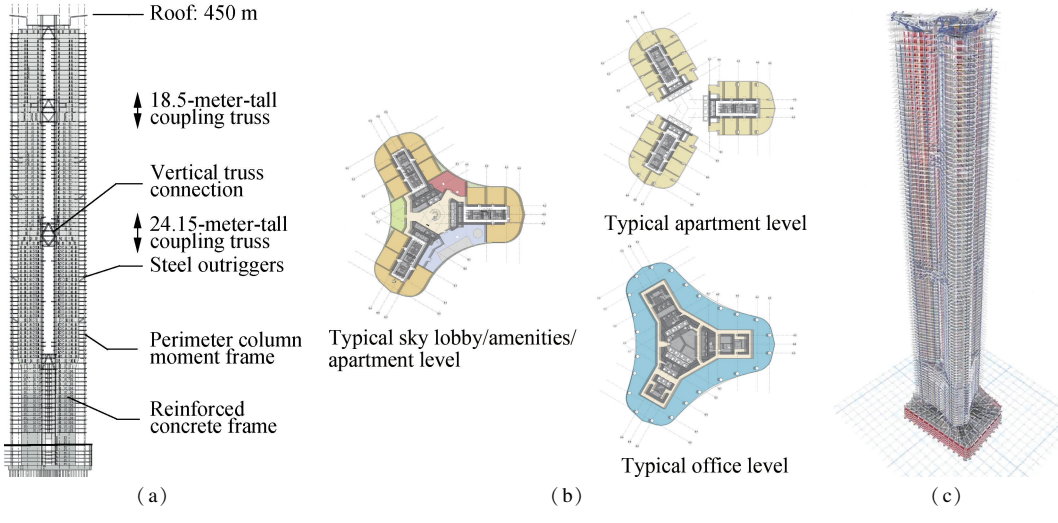

Fig. 1 Elevation and plane of Suzhou Supertall. (a) Overall elevation; (b) Planes of typical floors; (c) ETABS model

The plane layout can be categorized as a triangular layout in lower zones and a three-tower petal layout in higher zones. Ten refuge floors are spaced vertically at about 50 m apart, dividing the structure into 10 segments. The bottom two segments are office floors, while the other eight segments are apartment floors. The three-tower layout is interconnected through three service floors that belong to the apartment floor, located on the 46th-51st, 76th-79th, and 97th-100th floors. The reinforced concrete core tube extends from the raft to the roof, continuous moment frames are positioned around the office floors, and closed moment frames are arranged in each tower of the apartment floors. Connected trusses are located in three sky lobbies and the roof.

The core shear wall thickness and frame column dimensions within the structure progressively decrease from the base to the top. The shear wall thickness ranges from a maximum of 1 500 mm to a minimum of 300 mm. The frame columns, constructed with steel-reinforced concrete, exhibit dimensions ranging from a maximum of 1 800 mm × 650 mm to a minimum of 800 mm × 650 mm. For floors below 150 m, C80 concrete is utilized; for those between 150 and 250 m, C70 concrete is employed, while for heights exceeding 250 m, and C50-C60 concrete are used, respectively. The main bar consistently adheres to the HRB500 standard.

The seismic design specifications include a seismic design intensity of seven degrees, a seismic design group of Group 1, a site soil classification of Category Ⅲ, and a characteristic period of 0.55 s, which comes from the preliminary GEO report. The structure's seismic fortification category is Category B, and its damping ratio is 4.0%. The total mass of the structure is 4.3×10^5 t. The first three fundamental periods of this high-rise building are 8.49, 8.28, and 6.88 s, respectively, and the basic wind pressure of 50 a return is 0.45 kPa. The site roughness belongs to Category B, and the shape factor is 1.3.

2 Ground Motion Selection and Wind Load Simulation

2.1 Ground motion selection

Ground motion is a wide-frequency-band, nonstationary random vibration process with great uncertainty that is affected by various factors, such as site conditions, propagation paths, and seismogenic mechanisms. Different record inputs into the structure lead to great differences in the displacement and internal force of the structural system. Therefore, to ensure the reliability of the analysis results, ground motions must be reasonably selected according to specific standards.

Selection principles for ground motion records are proposed in FEMA P-695[25], as outlined in the following eight points:

1) The earthquake magnitude should be at least 6.5.

2) Earthquakes are induced by strike-slip or reverse sources.

3) Seismic recordings should be on soft rock or stiff soil sites.

4) The source-to-site distance should be greater than 10 km.

5) No more than two records should be taken from one earthquake for a record set.

6) The limits on PGA and PGV should be greater than $0.2g$ and greater than 15 cm/s, respectively.

7) Records should have a valid frequency content of at least 4 s.

8) Instruments located in a free-field location or on the ground floor of a small building should be used.

According to the US Federal Highway Administration[26], site characteristics include the shear wave velocity within the upper 30 m of the site, $v_{s,30}$, and the corresponding National Earthquake Hazard Reduction Program (NEHRP) Site Class. Because of differences in the site soil classification in seismic codes between China and USA, the approach proposed by Liu[27] is applied to interpret the soil characteristics according to Chinese specifications[28] and obtain the seismic records that meet the site soil classification of the structure.

Based on selection principles for ground motion records in FEMA P-695 with a consideration of the site characteristics of Suzhou Supertall, a set of 10 real ground motion records is chosen. These records will be employed in nonlinear dynamic analysis, supplying essential data for the vulnerability analysis. Only the first 90 s of the records are considered. Table 1 presents detailed information on the ground motion records. Fig. 2 depicts a comparison between the input record response spectrum and the design response spectrum as per Chinese specification[28], where T represents the period, and S_a signifies the spectral acceleration.

Table 1 Ground motion records

Number	Ground motion	Year	Station	Magnitude	$v_{s,30}$/(m·s^{-1})	NEHRP class
EQ1	Imperial Valley-06	1979	Delta	6.53	242	D
EQ2	Imperial Valley-06	1979	El Centro Array #11	6.53	196	D
EQ3	Superstition Hills-02	1987	El Centro Imp. Co. Cent	6.54	192	D
EQ4	Superstition Hills-02	1987	Imperial Valley Wildlife Liquefaction Array	6.54	179	D
EQ5	Kobe, Japan	1995	Fukushima	6.90	256	D
EQ6	Kobe, Japan	1995	Shin-Osaka	6.90	256	D
EQ7	Chi-Chi, Taiwan, China	1999	CHY101	7.62	259	D
EQ8	Hector Mine	1999	Bombay Beach Fire Station	7.13	257	D
EQ9	Tottori, Japan	2000	SMN005	6.61	182	D
EQ10	El Mayor-Cucapah, Mexico	2010	TAMAULIPAS	7.20	242	D

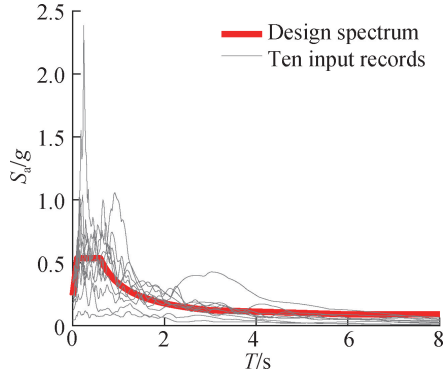

Fig. 2 Acceleration response spectrum of the input records

2.2 Wind load simulation

Downwind wind speed includes average wind speed and pulsating wind speed. Typically, the average wind speed is characterized over more than 10 min, whereas the pulsating wind speed is assessed over much shorter durations, typically ranging from a few seconds to several tens of seconds. Therefore, different methods are applied to describe these two aspects of wind speed.

2.2.1 Average wind speed

The impact of average wind speed on a structure can be simplified as a static force. According to the code[29], roughness Category B corresponds to a roughness coefficient of 0.15 and a gradient wind height of 350 m. The average wind speed at various heights above the ground is

$$v_z = v_{10}\left(\frac{z}{10}\right)^{0.15} \tag{1}$$

where v_z represents the average wind speed; z denotes the height above the ground; v_{10} stands for the average wind speed at a height of 10 m above the ground.

2.2.2 Pulsating wind speed

The pulsating wind speed has a shorter period and greater uncertainty than the average wind speed. To model the pulsating wind speed, the Davenport spectrum and the harmonic superposition method are employed[30-33]. In the Davenport spectrum, turbulence is considered constant along the height, and the power spectral density function is expressed as

$$\left.\begin{aligned} S_v(n) &= v_{10}^2\frac{4kx^2}{n(1+x^2)^{4/3}} \\ x &= \frac{1\,200n}{v_{10}} \end{aligned}\right\} \tag{2}$$

where $S_v(n)$ is the power spectrum of the pulsating wind speed; n signifies the pulsating wind frequency; k represents the ground roughness coefficient; x is the turbulence integral scale.

Fig. 3 displays the time-history simulation of pulsating wind speed based on an average wind speed of 15 m/s at a height of 10 m, demonstrating close agreement with the target spectrum.

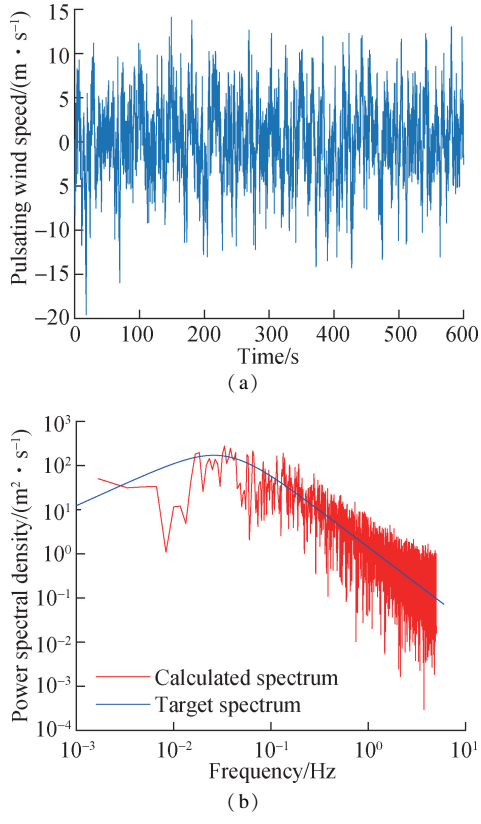

Fig. 3 Pulsating wind speed simulation based on an average wind speed of 15 m/s at a height of 10 m. (a) Time history of pulsating wind speed; (b) Comparison of power spectral density

2.2.3 Wind load calculation

The wind pressure specified in the code[29] is given by

$$\omega = \mu_s\frac{\rho}{2}(V+v)^2 \tag{3}$$

where ω is the wind pressure on the area surface; V and v represent the average and pulsating wind speed at the wind load action point, respectively; μ_s is the shape factor of the structure, taken as 1.3 as the project design data; ρ is the air density at the height of the action point, which is represented as

$$\rho = 1.25\times10^3\exp(-1\times10^{-4}z) \tag{4}$$

To improve computing efficiency, a structure with a roof height of 450 m is divided into nine computing areas along the height, and each area is 50 m high. The wind load's point of action is situated at the centroid of each area. The wind load in each calculation area of the structure is defined as

$$W = \omega A \tag{5}$$

where W is the wind load; A is the projected area of the windward surface of the computing area.

3 Vulnerability Analysis of Structures

3.1 Vulnerability analysis of a structure under individual earthquake actions

Structural vulnerability refers to the probability of surpassing a predefined damage level under a given disaster intensity[34–35]. The optimal choice of intensity measure R_{IM} and structural damage measure R_{DM} is crucial for vulnerability analysis. Within the framework of this study, the intensity measure is defined as the spectral acceleration corresponding to a structure's fundamental period for earthquake actions, $S_a(T_1,\xi)$, while the maximum inter-story drift θ_{max} is chosen as the structural damage measure. To achieve comparability with the result in Ref. [24], the corresponding median values for the maximum inter-story drift define performance levels: slight, moderate, severe, and collapse damage are represented by 1/500, 1/200, 1/100, and 1/50, respectively.

The probabilities of exceedance under individual earthquake actions are expressed as

$$P_f = P(C \leqslant R_{DM}) = \int P(C \leqslant R_{DM} \mid R_{DM} = x) f(x)\,\mathrm{d}x \tag{6}$$

where C denotes the structural capacity; P_f stands for the conditional probability of exceedance; $f(x)$ signifies the probability density function of R_{DM}. Under the lognormal distribution assumption for R_{DM} and C, P_f is approximated by[36]

$$P_f \approx 1 - \Phi\left(\frac{\ln\theta_c - \ln\theta_{max}}{\sqrt{\beta_D^2 + \beta_C^2}}\right) = \Phi\left(\frac{\ln\theta_{max} - \ln\theta_c}{\sqrt{\beta_D^2 + \beta_C^2}}\right) \tag{7}$$

where θ_c denotes the inter-story drift limit associated with distinct damage levels; β_C is the logarithmic standard deviation of the structural resistance capacity (assumed as 0.3); Φ represents the standard normal distribution function; β_D signifies the lognormal distribution standard deviation of the structure's disaster resistance requirement R_{DM} and is expressed as[8]

$$\beta_D \simeq \sqrt{\frac{\sum_{i=1}^{n} (\ln\theta_{max,i} - a - b\ln R_{IM})^2}{N-2}} \tag{8}$$

where N is the number of samples; $\theta_{max,i}$ represents the maximum inter-story drift of the i-th simulated sample.

The relationship between R_{DM} and R_{IM} approximately satisfies[37]

$$R_{DM} = \alpha R_{IM}^{\beta} \tag{9}$$

where α and β are constants.

Applying the natural logarithm to both sides of Eq. (9) gives

$$\ln R_{DM} = a + b\ln R_{IM} \tag{10}$$

where $a = \ln\alpha$ and $b = \beta$ are constants.

R_{IM} of 10 ground motion records in Table 1 is scaled to $0.02g$, $0.04g$, $0.06g$, $0.08g$, $0.10g$, and $0.12g$ before their application in nonlinear dynamic structural analysis. The results from the nonlinear dynamic analysis are then inserted into Eq. (10) for linear regression analysis, and the regression equation is obtained as

$$\ln\theta_{max} = -1.749 + 0.995\ln S_a(T_1,\xi) \tag{11}$$

By substituting Eq. (11) into Eq. (7), the probabilities of the structure reaching different damage states can be obtained as

$$P_f = \Phi\left[\frac{-1.749 + 0.995\ln S_a(T_1,\xi) - \ln\theta_c}{\sqrt{\beta_D^2 + \beta_C^2}}\right] \tag{12}$$

Using Eqs. (11) and (12), the probability demand model and vulnerability curve for the structure under individual earthquake actions are derived (see Fig. 4). This figure indicates that the regression curve of the demand model fits well with the structural response to seismic actions. As the ground motion intensity increases, the probabilities of reaching the four damage levels are observed to also increase. Under rare earthquake scenarios, the pro-

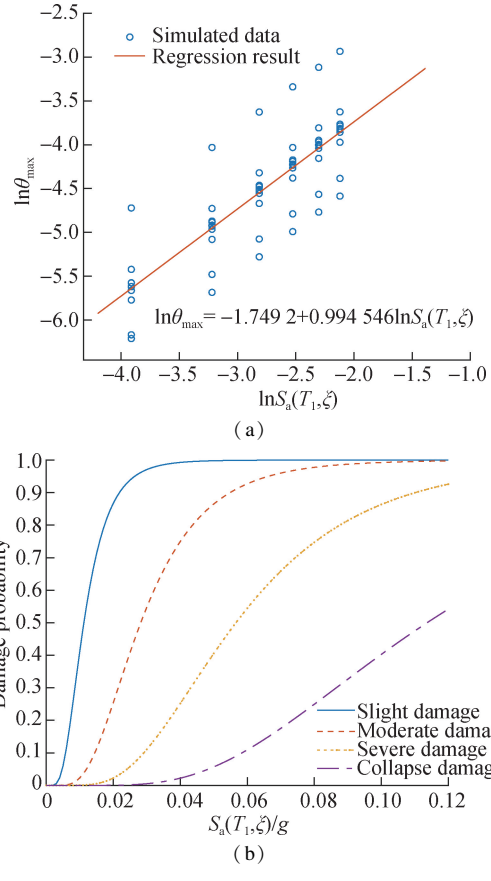

Fig. 4 Structural vulnerability analysis under seismic action alone. (a) Seismic demand model of the structure; (b) Seismic vulnerability curve

babilities of the structure suffering slight, moderate, severe, and collapse damage are 100%, 98.66%, 80.83%, and 31.89%, respectively.

3.2 Vulnerability analysis under combined earthquake-wind actions

Considering the structure damage probability under the combined earthquake-wind actions, the structural vulnerability function under multiple disaster scenarios is defined in Eq. (7) with the description of β_D provided as

$$\beta_D = \sqrt{\frac{\sum_{i=1}^{n} (\ln\theta_{\max,i} - a - b\ln R_{IM1} - c\ln R_{IM2})^2}{N-2}} \quad (13)$$

where R_{IM1} and R_{IM2} signify intensity measures for the seismic action and the wind load, respectively.

The multi-hazard probability demand model approximately satisfies

$$\ln R_{DM} = a + b\ln R_{IM1} + c\ln R_{IM2} \quad (14)$$

where c is a constant.

Within the framework of this study, R_{IM1} for the seismic action is defined as the spectral acceleration corresponding to the structure's fundamental period, $S_a(T_1, \xi)$, and is scaled to $0.02g$, $0.04g$, $0.06g$, $0.08g$, $0.10g$, and $0.12g$, respectively. R_{IM2} for the wind load is described as the average wind speed at a height of 10 m above the ground, v_{10}, and is scaled to 15, 20, 25, 30, 35, and 40 m/s, respectively. The maximum inter-story drift of the structure $\theta_{\max}$ is chosen as the DM. The wind load is initially calculated using Eqs. (3) and (5). Then, 360 combinations of the seismic action and the wind load of different intensities are obtained, which are subsequently input for nonlinear dynamic analysis. The results obtained are substituted into Eq. (14) for multiple linear regression analysis, and the regression equation is obtained as

$$\ln\theta_{\max} = -2.896 + 0.828\ln S_a(T_1,\xi) + 0.256\ln v_{10} \quad (15)$$

Fig. 5 presents the probability demand model for the structure under combined earthquake-wind influences. This figure illustrates that the regression surface of the demand model fits well with the response of the structure under the coupling action.

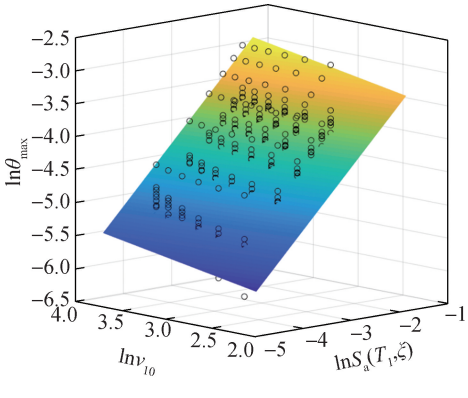

Fig. 5 Demand model for the structure subjected to the combined effects of earthquake and wind

By inserting Eq. (15) into Eq. (7), the probabilities of the structure attaining various damage levels are determined as

$$P_f = \Phi\left[\frac{-2.896 + 0.828\ln S_a(T_1,\xi) + 0.256\ln v_{10} - \ln\theta_c}{\sqrt{\beta_D^2 + \beta_C^2}}\right] \quad (16)$$

According to Eq. (16), the vulnerability surface for the structure under the earthquake-wind coupling excitations is drawn in Fig. 6. This figure depicts that when the structure is subjected to coupling actions, the vulnerability increases with the earthquake and wind intensity. For further quantitative analysis, Table 2 presents the probabilities of the structure exceeding the four damage levels under the earthquake-wind coupling excitations. In this table, the seismic action plays a dominant role in the structural damage in the four damage levels. With increasing earthquake intensity, the probabilities of the structure exceeding the four damage levels increase rapidly, while the increase in wind load intensity results in a slower growth in the probability of exceeding these levels. More precisely, at a maximum wind speed of 40 m/s, the probability of exceeding collapse damage within the range of the studied earthquake intensity increases by 0.67. However, at the maximum earthquake intensity, the probability of the structure exceeding collapse damage within the scope of the studied wind load intensity only increases by 0.21.

Table 3 summarizes the vulnerability of the super high-rise connected structure under individual rare earthquake actions and the combined actions of a rare earthquake and an average wind speed of 40 m/s. It is evident that when subjected to combined earthquake-wind actions, the probabilities of the structure reaching moderate, severe, and collapse damage are 99.77%, 91.56%, and 46.54%, respectively, representing an increase of 1.11%, 10.73%, and 14.65% respectively, compared to the case of rare earthquake actions alone. This comparison underscores the importance of wind load on the structure's performance, emphasizing that neglecting it could lead to an overestimation of the structure's safety and result in an unsafe condition.

To compare the multihazard vulnerability of super high-rise and high-rise connected structures[24], the probabilities of exceedance of two structures under the combined effects of a rare earthquake and an average wind speed of 40 m/s are presented in Table 4. The data indicate that compared to the high-rise connected structures, super high-

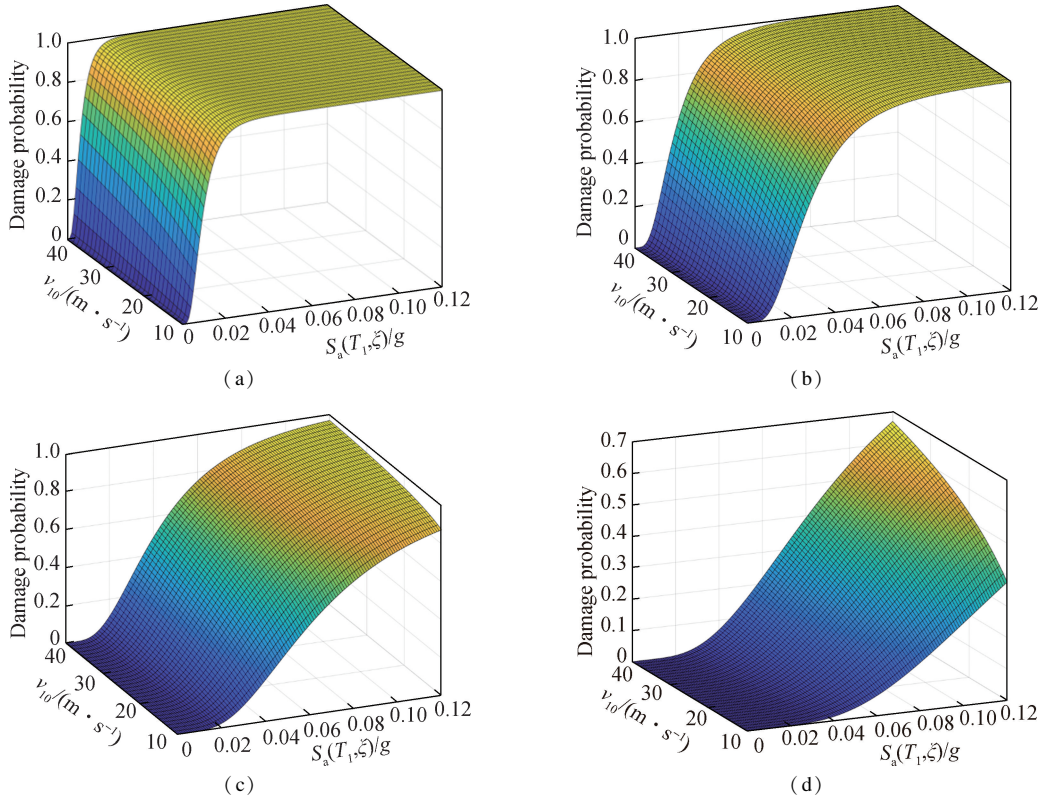

Fig. 6 Vulnerability surface under the combined earthquake-wind excitations. (a) Slight damage; (b) Moderate damage; (c) Severe damage; (d) Collapse damage

Table 2 Probabilities of exceedance under coupling actions of earthquake and wind

Damage level	Intensity of wind/(m · s^{-1})	Probability of exceedance for different earthquake intensities					
		0.02g	0.04g	0.06g	0.08g	0.10g	0.12g
Slight	15	0.95	1.00	1.00	1.00	1.00	1.00
	20	0.96	1.00	1.00	1.00	1.00	1.00
	25	0.97	1.00	1.00	1.00	1.00	1.00
	30	0.98	1.00	1.00	1.00	1.00	1.00
	35	0.98	1.00	1.00	1.00	1.00	1.00
	40	0.98	1.00	1.00	1.00	1.00	1.00
Moderate	15	0.38	0.82	0.95	0.98	0.99	1.00
	20	0.44	0.86	0.96	0.99	1.00	1.00
	25	0.49	0.88	0.97	0.99	1.00	1.00
	30	0.53	0.90	0.98	0.99	1.00	1.00
	35	0.56	0.91	0.98	1.00	1.00	1.00
	40	0.59	0.93	0.98	1.00	1.00	1.00
Severe	15	0.04	0.29	0.56	0.75	0.85	0.91
	20	0.05	0.35	0.62	0.79	0.89	0.94
	25	0.07	0.39	0.67	0.83	0.91	0.95
	30	0.08	0.43	0.70	0.85	0.92	0.96
	35	0.10	0.46	0.73	0.87	0.93	0.97
	40	0.11	0.49	0.75	0.88	0.94	0.97
Collapse	15	0.00	0.02	0.10	0.21	0.34	0.46
	20	0.00	0.03	0.12	0.26	0.40	0.52
	25	0.00	0.04	0.15	0.30	0.45	0.57
	30	0.00	0.05	0.18	0.33	0.48	0.61
	35	0.00	0.06	0.20	0.36	0.52	0.64
	40	0.00	0.07	0.22	0.39	0.55	0.67

Table 3 Comparison of vulnerability for super high-rise connected structure under rare earthquake actions alone and combined earthquake-wind actions %

Damage level	Probability of exceedance		Difference
	Combined earthquake-wind actions	Rare earthquake actions	
Slight	100	100	0
Moderate	99.77	98.66	1.11
Severe	91.56	80.83	10.73
Collapse	46.54	31.89	14.65

Table 4 Comparison of vulnerability between super high-rise and high-rise connected structures under combined earthquake-wind actions %

Damage level	Probability of exceedance		Difference
	Super high-rise connected structure	High-rise connected structure	
Slight	100	100	0
Moderate	99.77	99.50	0.27
Severe	91.56	85.30	6.26
Collapse	46.54	32.20	14.34

rise connected structures have higher probabilities of moderate, severe, and collapse damage by 0.27%, 6.26%, and 14.34%, respectively. This notable increase is primarily due to the super high-rise connected structures having lower lateral stiffness and more pronounced long-period vibration characteristics, rendering them more vulnerable to the combined earthquake-wind impacts.

Fig. 7 provides a comprehensive visualization of the changes in the probabilities of exceeding super high-rise connected structures under various intensities of combined earthquake-wind excitations. As depicted in this figure, under combined earthquake-wind actions, the probabilities of the structure exceeding the four failure states increase compared with that under the individual earthquake actions. However, the influence of wind load on the probabilities of exceedance differs among wind speeds. As shown in Figs. 7(a) and (b), when the wind speed is low, the impact of the wind load primarily elevates the structural probabilities of exceeding slight and moderate

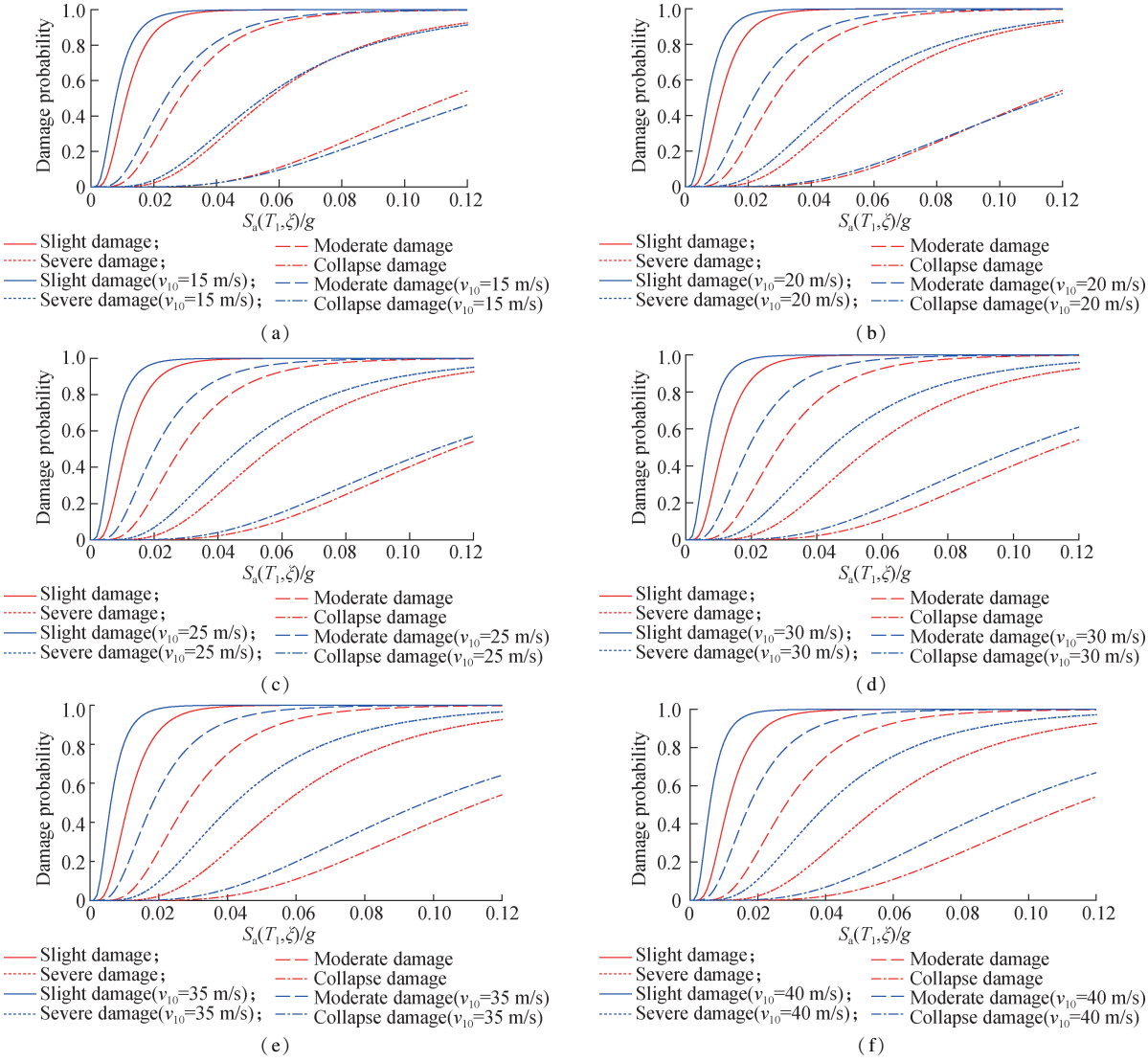

Fig. 7 Impact of wind loads on multi-hazard vulnerability of the structure. (a) v_{10} = 15 m/s; (b) v_{10} = 20 m/s; (c) v_{10} = 25 m/s; (d) v_{10} = 30 m/s; (e) v_{10} = 35 m/s; (f) v_{10} = 40 m/s

damage but has little effect on the probabilities of exceeding severe and collapse damage. Conversely, as illustrated in Figs. 7(e) and (f), at higher wind speeds, the actions of wind load considerably increase the structural probabilities of exceeding severe and collapse damage while exhibiting little impact on the probabilities of the structure exceeding slight and moderate damage.

4 Conclusions

1) The multihazard vulnerability of a structure under coupling earthquake-wind actions intensifies with increasing ground motion and wind load intensity. The seismic action primarily drives the probability of the structure exceeding damage levels. However, as the wind speed increases, the impact of wind load on the probabilities of exceedance becomes increasingly obvious. The actions of wind load mainly increase the probabilities of slight and moderate damage in the case of a small wind speed and mainly increase the probabilities of severe and collapse damage to the structure in the case of high wind speed.

2) The influence of wind load on structural damage should not be underestimated, as neglecting it could lead to an overestimation of the structure's performance, potentially resulting in an unsafe design. Under combined earthquake-wind actions, the probabilities of the structure suffering moderate, severe, and collapse damage are considerably higher than scenarios with seismic actions alone. When the wind speed reaches 40 m/s, the probabilities of the structure suffering these three damage states under rare earthquakes are 99.88%, 91.56%, and 46.54%, respectively, representing an increase of 1.22%, 10.73%, and 14.65% compared with that under rare earthquakes alone.

3) The vulnerability of super high-rise connected structures under combined earthquake-wind actions is more pronounced than that of high-rise connected structures. This greater vulnerability is mainly attributed to the smaller lateral stiffness and more long-period vibration shapes of super high-rise connected structures, and therefore, the structure is more susceptible to combined earthquake-wind actions. Compared with the high-rise connected structure studied by Yang et al., the probabilities of the super high-rise structure reaching the three damage states under the same combined actions are increased by 0.27%, 6.26%, and 14.34%, respectively.

References

[1] Ding J M, Wu H L, Zhao X. Current situation and discussion of structural design for super high-rise buildings above 250 m in China[J]. *Journal of Building Structures*, 2014, **35**(3): 1 −7. DOI: 10.14006/j.jzjgxb.2014.03.002. (in Chinese)

[2 Xie Y S, Xu Z D, Wang H. Occupant comfort evaluation of high-rise building under wind loads using LES[J]. *Journal of Southeast University (English Edition)*, 2023, **39**(2): 127 − 132. DOI: 10.3969/j.issn.1003-7985.2023.02.003.

[3] Zhang Z X, Chen Q J. A comparative study on long-period seismic responses for high-rise structures[J]. *Structure engineers*, 2009, **25**(4): 78 −84. DOI: 10.15935/j.cnki.jggcs.2009.04.020. (in Chinese)

[4] Cheng Y, Dong Y R, Bai G L, et al. IDA-based seismic vulnerability of high-rise frame-core tube structure subjected to multi-dimensional long-period ground motions[J]. *Journal of Building Engineering*, 2021, **43**: 102917. DOI: 10.1016/j.jobe.2021.102917.

[5] Jing F, Zhang L, Singh R P, et al. Quasi-coseismic variations and geosphere coupling associated with the strong 2023 Turkey earthquakes[J]. *Science of the Total Environment*, 2024, **907**:167963. DOI 10.1016/j.scitotenv.2023.167963.

[6] Jin S G, Han L, Cho J. Lower atmospheric anomalies following the 2008 Wenchuan Earthquake observed by GPS measurements[J]. *Journal of Atmospheric and Solar-terrestrial Physics*, 2011, **73**(7/8): 810 − 814. DOI: 10.1016/j.jastp.2011.01.023.

[7] Fujibe F. Localized strong winds associated with extensive fires in central Tokyo: Cases of the Great Kanto Earthquake (1923) and an air attack in World War Ⅱ (1945)[J]. *Journal of Wind Engineering and Industrial Aerodynamics*, 2018, **181**: 79 − 84. DOI: 10.1016/j.jweia.2018.08.016.

[8] Zheng X W, Li H N, Yang Y B, et al. Damage risk assessment of a high-rise building against multihazard of earthquake and strong wind with recorded data[J]. *Engineering Structures*, 2019, **200**:109697. DOI: 10.1016/j.engstruct.2019.109697.

[9] Xu L H, Liu Y Y, Xie X S. Performance study of steel frame self-centering braced tube structure under coupling action of earthquake and wind[J]. *Engineering Mechanics*, 2022, **39**(11): 186 − 195. DOI: 10.6052/j.issn.1000-4750.2021.07.0517. (in Chinese)

[10] Xie L L, Li X Y, Li A Q, et al. Fragility models of precast concrete shear walls with grouted sleeves[J]. *Journal of Southeast University (Natural Science Edition)*, 2021, **51**(6): 935 − 941. DOI: 10.3969/j.issn.1001-0505.2021.06.003. (in Chinese)

[11] Jiang H, Li C, Feng M Y, et al. Analysis on probabilistic seismic damage characteristics of dry joint prefabricated bridge pier based on kernel density estimation[J]. *Journal of Southeast University (Natural Science Edition)*, 2021, **51**(4): 566 − 574. DOI: 10.3969/j.issn.1001-0505.2021.04.003. (in Chinese)

[12] Shen H J, Wang H, Zheng W Z, et al. Analysis of critical directions of earthquake input of high-speed railway continuous girder bridges based on fragility analysis method[J]. *Journal of Southeast University (Natural Science Edition)*, 2019, **49**(5): 926 − 932. DOI: 10.3969/j.issn.1001-0505.2019.05.016. (in Chinese)

[13] Lu X L, Su N F, Zhou Y. IDA-based seismic vulnerabil-

ity analysis of a complex high-rise structure[J]. *Journal of Earthquake Engineering and Engineering Vibration*, 2012, **32**(5): 19 - 25. DOI: 10.13197/j.eeev.2012.05.017. (in Chinese)

[14] Zhou Y, Lu X L, Bu Y. Application of incremental dynamic analysis to seismic evaluation of hybrid structure [J]. *Journal of Tongji University (Natural Science)*, 2010, **38**(2): 183 - 187, 193. DOI: 10.3969/j.issn.0253-374x.2010.02.006. (in Chinese)

[15] Wang F, Li H N. Seismic damage assessment procedure of structures by using simplified IDA[J]. *Engineering Mechanics*, 2018, **35**(12): 194 - 202. DOI: 10.6052/j.issn.1000-4750.2018.04.0246. (in Chinese)

[16] Li H N, Li G, Zheng X W, et al. Research progress in engineering structures subject to multiple hazards[J]. *China Civil Engineering Journal*, 2021, **54**(5): 1 - 14. DOI: 10.15951/j.tmgcxb.2021.05.001. (in Chinese)

[17] Wang Z J. *Multi-hazard vulnerability analysis of isolated high-rise frame-shear-wall under wind-earthquake action* [D]. Lanzhou: Lanzhou University of Technology, 2022. (in Chinese)

[18] Zhou Y, Shan H W, Xing L L, et al. Study on vulnerability of Shanghai Tower under combined actions of wind and earthquake [J]. *World Earthquake Engineering*, 2020, **36**(2): 1 - 11. DOI: 10.3969/j.issn.1007-6069.2020.02.001. (in Chinese)

[19] Zheng X W, Li H N, Gardoni P. Hybrid Bayesian-Copula-based risk assessment for tall buildings subject to wind loads considering various uncertainties[J]. *Reliability Engineering & System Safety*, 2023, **233**: 109100. DOI: 10.1016/j.ress.2023.109100.

[20] Zheng X W, Li H N, Shi Z Q. Hybrid AI-Bayesian-based demand models and fragility estimates for tall buildings against multi-hazard of earthquakes and winds[J]. *Thin-Walled Structures*, 2023, **187**: 110749. DOI: 10.1016/j.tws.2023.110749.

[21] Zheng X W, Li H N, Gardoni P. Reliability-based design approach for high-rise buildings subject to earthquakes and strong winds[J]. *Engineering Structures*, 2021, **244**: 112771. DOI: 10.1016/j.engstruct.2021.112771.

[22] Zheng X W, Li H N, Gardoni P. Probabilistic seismic demand models and life-cycle fragility estimates for high-rise buildings[J]. *ASCE—Journal of Structural Engineering*, 2021, **147**(12): 04021216. DOI: 10.1061/(ASCE)ST.1943-541X.0003216.

[23] Zheng X W, Li H N. Life-cycle failure probability analysis of deteriorated RC bridges under multiple hazards of earthquakes and strong winds[J]. *Earthquake Engineering and Engineering Vibration*, 2022, **21**(3): 811 - 823. DOI: 10.1007/s11803-022-2111-6.

[24] Yang L S, Chen X, Tan L H, et al. Study on joint vulnerability analysis method of conjoined high-rise buildings under combined actions of earthquake and wind[J]. *Chinese Journal of Computational Mechanics*, 2023, **40**(6): 902 - 911. DOI: 10.7511/jslx20220610002. (in Chinese).

[25] Federal Emergency Management Agency. Quantification of building seismic performance factors[R]. Washington DC, USA: FEMA P-695, 2009.

[26] US Department of Transportation Federal Highway Administration. LRFD seismic analysis and design of transportation geotechnical features and structural foundations reference manual[R]. Washington DC, USA: Federal Highway Administration, 2011.

[27] Liu X T. *Research on probabilistic response spectrum and ground motion parameter spectrum of class Ⅱ site* [D]. Qingdao: Qingdao Technological University, 2018. (in Chinese)

[28] Ministry of Housing and Urban-Rural Development of People's Republic of China. Code for seismic design of buildings (2016 version): GB 50011—2010[S]. Beijing: China Architecture & Building Press, 2016. (in Chinese)

[29] Ministry of Housing and Urban-Rural Development of People's Republic of China. Load code for the design of building structures: GB 50009—2012[S]. Beijing: China Architecture & Building Press, 2012. (in Chinese)

[30] Yuan B, Zeng M H, Li X Z. Base on FFT method to simulate fluctuating wind and Matlab realization[J]. *Sichuan Building Science*, 2013, **39**(5): 29 - 32, 42. DOI: 10.3969/j.issn.1008-1933.2013.05.007. (in Chinese)

[31] Sun Z. *Computer simulation and analysis of wind loading of structures*[D]. Nanjing: Nanjing University of Aeronautics and Astronautics, 2007. (in Chinese)

[32] Liu X L, Zhou Y. Numerical simulation methods of wind load[J]. *Industrial Construction*, 2005(5): 81 - 84. DOI: 10.3321/j.issn:1000-8993.2005.05.021. (in Chinese)

[33] Yan S, Zheng W. Wind load simulation by superposition of harmonic[J]. *Journal of Shenyang Jianzhu University (Natural Science)*, 2005(1): 1 - 4. DOI: 10.3969/j.issn.2095-1922.2005.01.001. (in Chinese)

[34] Lu D G, Li X P, Wang G Y. Global seismic vulnerability analysis of structures based on reliability and performance[J]. *Journal of Natural Disasters*, 2006(2): 107 - 114. DOI: 10.3969/j.issn.1004-4574.2006.02.018. (in Chinese)

[35] Lu G Y, Wang K H, Zhang PP. Performance-based system seismic assessment for long-span suspension bridges under two-level seismic hazard[J]. *Journal of Southeast University (English Edition)*, 2019, **35**(4): 464 - 475. DOI: 10.3969/j.issn.1003-7985.2019.04.009.

[36] Wen Y, Ellingwood B R, Bracci J M. Vulnerability function framework for consequence-based engineering [R]. Chicago, IL, USA: MAE Center, 2004.

[37] Cornell C A, Jalayer F, Hamburger R O, et al. Probabilistic basis for 2000 SAC Federal Emergency Management Agency steel moment frame guidelines[J]. *Journal of Structural Engineering*, 2002, **128**(4): 526 - 533. DOI: 10.1061/(ASCE)0733-9445(2002)128:4(526).

地震和风耦合作用下超高层连体结构易损性分析

鲁　正[1,2]　严德裕[1]　周梦瑶[1]　赵　昕[3]　赵一青[4]

([1] 同济大学结构防灾减灾工程系, 上海 200092)
([2] 同济大学土木工程防灾减灾全国重点实验室, 上海 200092)
([3] 同济大学建筑设计研究院(集团)有限公司, 上海 200092)
([4] 中海企业发展集团有限公司, 深圳 518048)

摘要:为探究超高层连体结构在多灾害耦合作用下的设计与安全性能,以苏州超塔为例,开展地震和风耦合作用下的多灾害易损性分析. 根据设计资料建立结构有限元模型,分别开展结构在地震作用下以及地震和风耦合作用下的易损性分析,探究结构在多灾害耦合作用下的响应规律. 结果表明,地震和风耦合作用下结构联合易损性随着地震动和风荷载强度的增大而增加,且地震动对结构的破坏占主导作用. 地震与风耦合作用时结构达到中等破坏、严重破坏和倒塌破坏的概率均比仅地震作用时有所增加. 当风速达到 40 m/s 时,结构在罕遇地震下达到 3 种破坏状态的概率分别为 99.77%、91.56% 和 46.54%,相比于仅罕遇地震作用下分别提高了 1.11%、10.73% 和 14.65%,相比于一般高层连体结构在同样的灾害耦合作用下分别提高了0.27%、6.26% 和 14.34%.

关键词:超高层;连体结构;多灾害;易损性;地震;风荷载;耦合作用;苏州超塔

中图分类号:TU973.2